Applied Catalysis B: Environmental 230 (2018) 135–144

Contents lists available at ScienceDirect

Applied Catalysis B: Environmental

journal homepage: www.elsevier.com/locate/apcatb

# $Ru_xCe_{1-x}O_{2-y}$ nanoparticles deposited on functionalized $\gamma$-$Al_2O_3$ as a thermally stable oxidation catalyst

Karolina A. Ledwa[a,*], Mirosława Pawlyta[b], Leszek Kępiński[a]

[a] Polish Academy of Sciences, Institute of Low Temperature and Structure Research, ul. Okólna 2, 50-422 Wrocław, Poland
[b] Silesian University of Technology, Institute of Engineering Materials and Biomaterials, ul. Konarskiego 18A, 44-100 Gliwice, Poland

ARTICLE INFO

*Keywords:*
$Ru_xCe_{1-x}O_{2-y}$ on alumina
Soot oxidation
Propane oxidation
Thermal stability
Ru doped ceria

ABSTRACT

Structural stability of ceria in catalysts used for reactions occurring at elevated temperatures is an important technological problem. In this work, we propose a simple method that should improve the thermal stability of Ru doped ceria nanoparticles supported on alumina.

Nanosized (≤5 nm), ruthenium doped ceria particles were synthesized by the reverse microemulsion method and then deposited on the functionalized $\gamma$-$Al_2O_3$ support. Obtained catalysts were investigated using a wide range of characterization methods (e.g. XRD, HRTEM, STEM-HAADF, $H_2$-TPR, XPS) to determine the dispersion and stability of ceria in the oxidizing and reducing atmosphere. The catalytic activity of the samples was tested in the reaction of soot and propane combustion.

It has been shown that covering of $\gamma$-$Al_2O_3$ support with a monolayer of decanoic acid enabled uniform dispersion of $Ru_xCe_{1-x}O_{2-y}$ nanoparticles and their very high resistance against sintering up to 800 °C in the oxidizing and especially in the reducing atmosphere. The ceria particles show also high reducibility at the low-temperature range (<500 °C), what positively influences on their catalytic activity in the oxidation processes. $Ru_{0.05}Ce_{0.95}O_{2-y}$ deposited on the functionalized alumina is an active and stable catalyst for total oxidation of soot ($T_{50}$ = 487 °C) and propane ($T_{50}$ = 225 °C).

## 1. Introduction

Cerium oxide is a very important catalytic material due to its unique properties, such as high oxygen storage capacity and mobility of the oxygen ions in the ceria lattice, which determine its high activity in many important catalytic processes [1–5]. Unfortunately, this material has one significant drawback, namely a tendency to sintering at high temperatures. This phenomenon still hinders a widespread commercial application of ceria containing systems.

In literature, there are few methods to enhance dispersion and to prevent sintering of the ceria nanoparticles at high temperatures. Most common and very effective method is stabilization of the ceria nanoparticles on high surface area supports, such as alumina [6–9] or silica [10].

In recent years, the interest in precious metals substituted oxides as active catalysts has increased substantially. $CeO_2$ nanoparticles with a fraction of cerium ions substituted by different metal ions were successfully obtained using various methods, e.g., the reverse microemulsion [11,12], solution combustion [13–15] or hydrothermal [16]. It was shown, that the Ce−O bonds are weakened by the presence of metal ions in ceria structure, making the surface more reducible. The interaction of the dopants with ceria is one of the main factors determining the reactivity of such systems. Incorporation of noble metal ions, e.g., ruthenium or rhodium, in the ceria lattice, enhances the dispersion of mixed oxide and its thermal stability against sintering. Such systems also show higher catalytic activity in oxidation reactions than the pure ceria [11,15].

In our previous work, we developed a new, efficient method for synthesis of the catalytic systems containing hydrophobic cerium oxide nanoparticles on $\gamma$-alumina support with surface functionalized by adsorption of a monolayer of decanoic acid [6]. The method was based on the idea of Cargnello et al. [17], who used octylsiloxane modified alumina as the support for $Pd@CeO_2$ particles (Pd encapsulated in ceria shell). Our method enables elimination of the problem with the hydrophobic surface of nanoparticles obtained by the reverse microemulsion method, which tends to agglomerate on hydrophilic alumina surface, but contrary to [17] avoids introducing silicon into the samples [6]. In the present study, we use this method to synthesize $Ru_xCe_{1-x}O_{2-y}/\gamma$-$Al_2O_3$ systems ($x \leq 0.075$), potentially active and stable oxidation catalysts. The aim of the work was predominantly a study of

* Corresponding author.
*E-mail address:* K.Ledwa@int.pan.wroc.pl (K.A. Ledwa).

https://doi.org/10.1016/j.apcatb.2018.02.037
Received 15 December 2017; Received in revised form 9 February 2018; Accepted 14 February 2018
Available online 15 February 2018

microstructure and stability of the systems in various atmospheres, as well as examine of its activity in the oxidizing reactions. Ru-containing catalysts are known as active for soot [11,18], and propane oxidation [19–21], thus we choose these processes to check the activity and durability of the obtained systems. Since ruthenium is more than ten times cheaper than Pt or Pd, traditional oxidation catalysts, its possible application would be highly advantageous.

## 2. Experimental

### 2.1. Materials

Aeroxide Alu-C ($S_{BET}$ = 102 $m^2/g$), produced by Evonik-Degussa company, was used as a catalyst support. Cyclohexane (99%), 1-pentanol (98,5%), n-hexane (95%), ethanol (96%), and Triton X-100 were obtained from POCH. Decanoic acid (98%), tetramethylammonium hydroxide (25% wt. water solution) and cerium (III) nitrate hexahydrate (99,5%) were obtained from Sigma Aldrich. Ruthenium nitrate solution (11% wt. of ruthenium ions in nitric acid) was obtained from Mennica Metale Szlachetne.

### 2.2. Synthesis

Functionalization of the alumina support was done by adsorption of a monolayer of decanoic acid on its surface, using the method described in our previous paper [6]. 0.125 g of decanoic acid was dissolved in 40 $cm^3$ of n-hexadecane. Then 2.5 g of Alu-C was added to the solution and the mixture was stirred at room temperature for 30 min. In the next step, the obtained hydrophobic support was purified using hexane and ethanol and then dried in the air at 60 °C for 20 h. The obtained material is assigned as $\gamma$-$Al_2O_3$(fn).

The $Ru_xCe_{1-x}O_{2-y}$ nanoparticles (x = 0.025; 0.05; 0.075) were obtained using reverse microemulsion method described elsewhere [6,11]. For details see Supplementary material. The functionalized alumina was added to 25 $cm^3$ of the suspension of $Ru_xCe_{1-x}O_{2-y}$ in cyclohexane to get the (Ce + Ru)/Al molar ratio equal to 1/10 (25% wt. of $Ru_xCe_{1-x}O_{2-y}$ on $\gamma$-$Al_2O_3$). The amount of functionalized support required to obtain this concentration was determined using the method described elsewhere [6]. The mixture was stirred for 20 h at RT to enable deposition of doped ceria nanoparticles on the support. The samples were dried at 60 °C for 24 h and then heated in air at 550 °C for 3 h to clean up the organic residues.

For comparison, the $Ru_xCe_{1-x}O_{2-y}$ nanoparticles were deposited in a similar way on bare (non-functionalized) $\gamma$-$Al_2O_3$. Analogous undoped $CeO_2$ containing systems were also synthesized as reference samples.

### 2.3. Characterization of catalysts

Fourier transform infrared (FTIR) measurements were performed to check for the possible presence of organic residues in the obtained catalysts. FTIR spectra were acquired for the powder samples, pressed in KBr pellet, using Biorad 575C FT-IR spectrometer with spectral resolution 2 $cm^{-1}$.

The atomic Ru/Ce/Al ratio in the samples and their chemical homogeneity were studied by energy dispersive spectroscopy (EDS) (EDAX Genesis XM4 spectrometer installed on FEI NovaNanoSEM 230 microscope).

The phase composition and mean crystallite size of nanoparticles in the samples were determined by XRD (X'Pert PRO PANalytical powder diffractometer, Cu $K_\alpha$ radiation). X'Pert HighScore Plus program was used for display and analyze the diffraction patterns, including the full profile fitting procedure.

The microstructure of the samples was investigated with a Philips CM-20 SuperTwin TEM microscope, operating at 160 kV and providing 0.25 nm resolution. HAADF images were obtained with FEI S/TEM TITAN operating at 300 kV, equipped with EDS spectrometer. Specimens were prepared by dispersing a small amount of the sample in methanol and putting a droplet of the suspension on a microscope copper grid covered with carbon. Samples were then dried and purified in plasma cleaner. Samples after reduction in a hydrogen atmosphere, because of their sensibility, were prepared by putting a small amount of dry sample on the microscopic grid.

Raman spectroscopy was used to check for the possible presence of amorphous Ru oxide, which cannot be detected using XRD method. Spectra were recorded with Renishaw InVia Raman spectrometer equipped with a confocal DM 2500 Leica optical microscope, a CCD as a detector, Eclipse filter, a diode laser operating at 830 nm.

The specific surface area and porosity of the solid samples were determined by nitrogen adsorption at 77 K (Micrometrics ASAP 2020 Surface Area and Porosity Analyzer) by applying the BET method. Before the measurement, the samples (150 mg) were degassed by heating in vacuum at 250 °C for 4 h.

The surface composition and chemical state of the samples were determined by X-ray photoelectron spectroscopy. For two systems: $CeO_2$ and $Ru_{0.05}Ce_{0.95}O_{2-y}$ deposited on $\gamma$-$Al_2O_3$(fn), the following measurement cycles were performed: (1) measurement after purifying *in situ* in oxygen at 500 °C for 30 min and (2) measurement after reduction *in situ* in the $H_2$ atmosphere at 500 °C for 1 h. XPS spectrum of a fresh sample containing ruthenium was also acquired, to check for possible changes in the structure during the purifying process. The heating rate was 10 °C/min in all these treatments, and heating was performed at a gas pressure equal to 1 bar. The spectra were acquired under high vacuum ($2 \cdot 10^{-10}$ mbar) at room temperature, using a monochromatized Al $K_\alpha$ X-ray source (1486.6 eV–300 W) and a hemispherical analyzer (SCIENTA EW 3000) working with the pass energy 200 eV. The energy resolution, determined based on FWHM of the Ag $3d_{5/2}$ line, was 0.6 eV. An electron flood source was applied to neutralize the surface charges. The binding energies were calculated with reference to the line of Al 2p at 75 eV, characteristic for aluminum in the oxide form. Calculations were performed with CasaXPS software.

Temperature programmed reduction ($H_2$-TPR) measurements were performed by heating the samples (10 °C/min) up to 1000 °C in $H_2$ (5% vol.)/Ar flow (30 $cm^3$/min.) using AutoChem II 2920 apparatus. Before TPR measurements were accomplished, the samples were treated in $O_2$ (1% vol.)/He at 500 °C for 30 min to clean the surface.

Thermal stability of the obtained systems was investigated by heating the as-prepared samples in the tube furnace at different temperatures in oxidizing (air) or reducing ($H_2$ 99.95%) atmosphere for 1 h or 3 h. The heating rate was equal to 5 °C/min After the $H_2$ treatments, the samples were flushed for 1h in pure Ar (99.999%) to avoid rapid oxidation.

Thermogravimetric analysis (TGA) (Derivatograph TG-DTA, MOM Budapest) was used to determine the activity of the catalysts in soot oxidation process. Samples were prepared in a "tight contact" mode by grinding in a mortar 130 mg of the catalyst containing ~25 wt.% of the active mixed oxide (or 32.5 mg of unsupported oxide, where the active phase consists 100% wt.) with 65 mg of soot. Powder samples (190 mg of the prepared mixture with supported oxides, and 82 mg of the mixture with unsupported oxides) were placed in a corundum crucible and heated in air up to 650 °C, with a heating rate equal to 5 °C/min. For each sample, three oxidation cycles were performed to determine the stability of catalyst in the process.

Propane oxidation test reaction was carried out in a fixed-bed flow reactor [22], made of quartz tubing of 10 mm inner diameter and a programmable furnace. The catalyst (100 mg), previously additionally purified by heating at 500 °C in oxygen for 30 min, was activated in the gas mixture (5000 vppm propane in the air with a flow rate of 100 $cm^3$/min) by heating up to 150 °C (the heating rate of 3 °C/min) and stabilized at this temperature for 1 h. Measurements were performed stepwise at the temperature in the range of 150–400 °C. The reaction products were analyzed using a gas chromatograph (Perkin-Elmer ARNEL Clarus 500) equipped with thermal conductivity and flame ionization

detectors at each temperature until steady state activity was obtained.

Structure and morphology measurements for the samples after catalytic processes were performed similarly as for the as-prepared samples.

## 3. Results and discussion

### 3.1. Dispersion and structure of as-prepared samples

FTIR spectra of the as-prepared samples revealed no bands near 2900 $cm^{-1}$ assigned to −CH groups [23] (Fig. S1 – Supplementary material), indicating that the pretreatment procedure was sufficient to remove remains of the organic phase. Detailed analysis of the FTIR spectra of such systems was done in our previous paper [6]. Metal content in the as-prepared samples, measured using SEM-EDS method is close to the nominal one (Table S1 and Fig. S2 in Supplementary material).

Fig. S3 (Supplementary material) presents XRD patterns of the as-prepared $Ru_xCe_{1-x}O_{2-y}$/ γ-$Al_2O_3$(fn) samples (x = 0; 0.025; 0.05; 0.075). The diffractograms for samples with x = 0–0.05 are very similar, and contain, in addition to γ-$Al_2O_3$, strong reflections corresponding to the fluorite structure of $CeO_2$ (Fig. S4 – Supplementary material) [24]. Average crystallite sizes of ceria calculated by using the full profile fitting procedure are presented in Table 1. For all $Ru_xCe_{1-x}O_{2-y}$/γ-$Al_2O_3$(fn) samples the sizes are similar (3–4 nm) and are slightly smaller than those for the reference samples deposited on bare alumina. Average crystallite sizes in the unsupported oxide are much larger, what evidences the stabilizing role of the support. For the sample with the highest Ru content (x = 0.075) reflections of $RuO_2$ occur, indicating that certain part of Ru is located outside the ceria lattice. For the unsupported $Ru_xCe_{1-x}O_{2-y}$, ruthenium oxide reflections are observed for sample with the much higher dopant concentration (x = 0.125) (Fig. S5 – Supplementary material). Kurnatowska et al. reported the maximal concentration of ruthenium ions in the ceria structure equal to x = 0.13 for unsupported nanoparticles, obtained by similar reverse microemulsion method and calcined at 500 °C in $O_2$ for 2 h [11]. Similar results (x = 0.11 and 0.15) were reported by Singh et al. for $Ru_xCe_{1-x}O_{2-y}$ nanoparticles prepared by various methods [21,25]. The difference can be due to the smaller sizes of the oxide particles obtained in our supported systems, predominantly to 2–4 nm (Fig. 1, Table 1). The lower solubility of Ru in the ceria lattice in our case can be also due to the relatively high temperature of the samples pretreatment (550 °C in the air). Kurnatowska et al. [11] reported a partial decomposition of $Ce_{0.89}Ru_{0.11}O_2$ at 600 °C in an oxidizing atmosphere with the formation of crystalline $RuO_2$. The maximal concentration of Ru in $CeO_2$ at 550 °C equal to x = 0.05, has been reported by Sharma et al. [26] and was close to that predicted by Li et al. [27] for a meta-stable regime of the ruthenium-cerium oxide solid solution at this temperature. Further, in the paper, we will restrict our interest mostly to samples with Ru content x = 0.05.

Significant improvement in the dispersion of $Ru_xCe_{1-x}O_{2-y}$ particles on the functionalized alumina, as compared with bare alumina, is seen in STEM micrographs. Fig. 1 presents a representative STEM-HAADF image of the as-prepared $Ru_{0.05}Ce_{0.95}O_{2-y}$/γ-$Al_2O_3$(fn) sample. As HAADF detector collects elastically high-angle scattered electrons, the image intensity is therefore proportional to the integral of $Z^2$ (atomic number Z raised to a power 2) along the beam direction and recorded HAADF image directly present chemical contrast. Therefore, bright spots on the images can be identified as the Ru doped ceria particles, while the gray area as alumina support. That conclusion was also confirmed by the EDS. The particles with sizes 2–5 nm and narrow particle size distribution (PSD) are homogeneously dispersed on the support, mostly as isolated items (Fig. 1). By contrast, many large agglomerates of ceria particles are observed on nonfunctionalized alumina (Fig. S6 – Supplementary material). Such effect is also observed for samples with other Ru concentration, including pure $CeO_2$ [6].

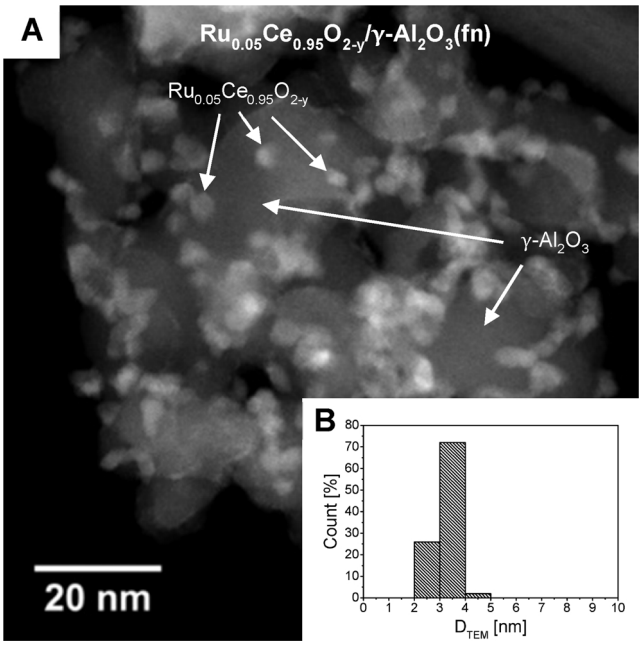


**Fig. 1.** (A) Example of the STEM-HAADF image of as-prepared $Ru_{0.05}Ce_{0.95}O_{2-y}$/ γ-$Al_2O_3$(fn), (B) particle size distribution of the oxide particles calculated from HRTEM images.

**Table 1**
Specific surface area ($S_{BET}$), total pore volume ($V_{BET}$), average pore width ($L_{BET}$) and average crystallite sizes calculated from the XRD patterns for the as-prepared samples.

| Sample | $S_{BET}$ [$m^2$/g] | $V_{BET}$ [$cm^3$/g] | $L_{BET}$ [nm] | $D_{XRD}$ [nm] |
|---|---|---|---|---|
| $Ru_{0.025}Ce_{0.975}O_{2-y}$ | – | – | – | 5.5 |
| $Ru_{0.025}Ce_{0.975}O_{2-y}$/γ-$Al_2O_3$ | 105 | 0.60 | 23 | 4.0 |
| $Ru_{0.025}Ce_{0.975}O_{2-y}$/γ-$Al_2O_3$(fn) | 114 | 0.65 | 23 | 3.6 |
| $Ru_{0.05}Ce_{0.95}O_{2-y}$ | – | – | – | 5.3 |
| $Ru_{0.05}Ce_{0.95}O_{2-y}$/γ-$Al_2O_3$ | 111 | 0.65 | 23 | 3.7 |
| $Ru_{0.05}Ce_{0.95}O_{2-y}$/γ-$Al_2O_3$(fn) | 119 | 0.67 | 23 | 3.3 |

Specific surface area ($S_{BET}$) of the sample with oxide particles deposited on functionalized supports (Table 1) is about 8% higher than for doped ceria on bare alumina. It also confirms the positive effect of the support functionalization on ceria dispersion.

Fig. 2 depicts the Raman spectra of representative samples. For the as-prepared $CeO_2$/ γ-$Al_2O_3$(fn) sample, strong (458 $cm^{-1}$) and weak (600 $cm^{-1}$) bands are visible. The band near 460 $cm^{-1}$ is attributed to the characteristic $F_{2g}$ vibrational mode of the fluorite structure of $CeO_2$. It can be considered as the symmetrical stretching vibration of the oxygen atoms around cerium ions [9]. The weak band at 600 $cm^{-1}$ is related to the oxygen vacancies caused by the presence of small amount of $Ce^{3+}$ ions in the ceria structure [20]. For the as-prepared $Ru_{0.05}Ce_{0.95}O_{2-y}$/γ-$Al_2O_3$(fn) sample, three other bands are present in addition to the 460 and 600 $cm^{-1}$ bands mentioned above. The bands at 700 $cm^{-1}$ and 970 $cm^{-1}$ can be assigned to the surface Ru−O−Ce species [28–31] and the broad band between 220 and 380 $cm^{-1}$ probably to the second-order transverse acoustic mode (2TA) [30,31]. Characteristic Raman bands of the $RuO_2$ phase at 523, 646 and 710 $cm^{-1}$ are not observed, presumably due to very low concentration or absence of this phase in the sample [32].

### 3.2. Thermal stability

Thermal stability of the samples was evaluated by studying the effect of heating in air or in hydrogen at a temperature up to 1000 °C on

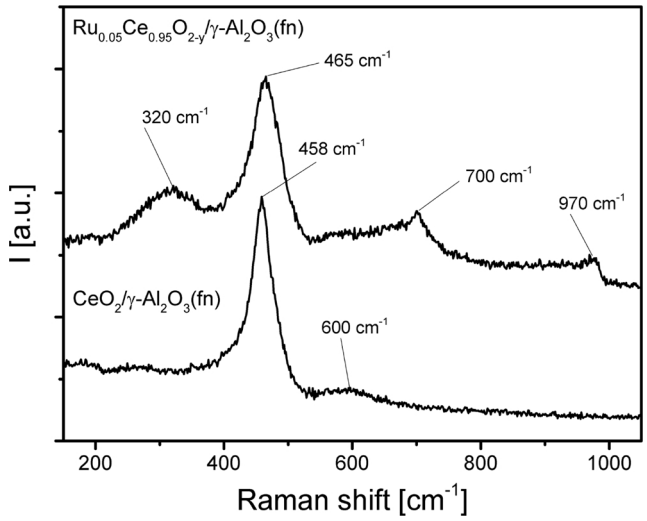


**Fig. 2.** Raman spectra of the as-prepared samples.

morphology and structure of the ceria phase.

Fig. 3 presents XRD patterns of $Ru_{0.05}Ce_{0.95}O_{2-y}/\gamma\text{-}Al_2O_3$(fn) heated in air at various temperatures. Up to 800 °C, the width of the ceria reflections changes only slightly, indicating high stability of the system against sintering at these conditions. However, weak reflections of the $RuO_2$ phase appear already at 700 °C, indicating rather weak bonding of the ruthenium ions in the $CeO_2$ lattice [33]. Interestingly, the intensity of $RuO_2$ reflections is almost the same after heating at 800 °C but decreases at 900 °C, and the reflections disappear at 1000 °C. It can be due to the re-entry of ruthenium ions in the ceria lattice, which was reported at high temperatures in oxidizing conditions [27].

The effect of prolonged (3 h) heating in the air at 800 °C on the morphology of ceria phase is presented in Fig. 4 and in the Supporting material in Fig. S7 and Table S2. The process causes the severe broadening of PSDs of ceria and its shift to the higher sizes, particularly for unsupported oxide. For the supported ceria, the effect is much weaker, especially for functionalized alumina. There is a good correspondence between the mean particle size measured from TEM and obtained from XRD (Table S2). No profound effect of Ru content on the sintering of ceria is observed.

Fig. 5 presents the effect of heat treatment in hydrogen at various temperatures on the XRD pattern $Ru_{0.05}Ce_{0.95}O_{2-y}/\gamma\text{-}Al_2O_3$(fn).

No noticeable sintering of the fluorite phase is observed up to 800 °C, what proves the high stability of the system. The average crystallite size increases slightly from 3.5 to 4.7 nm (Table 2). At 900 °C a new, cerium aluminate phase forms by the reaction of the reduced ceria with the alumina support [6,24,34,35]. The intensity of $CeAlO_3$ reflections (♦) is high and increases with the temperature of heating at the expense of ceria. Weak reflection corresponding to the strongest Ru (101) (♣) appears however in the XRD pattern at 500 °C and remains almost constant up to 1000 °C.

The Ru metallic particles could hardly be detected in HRTEM images because of their small size (few nm) and similar contrast from the ceria phase. Moreover, Ru is easily oxidized when the samples are exposed to air before the TEM study. Thus, the results related to the metallic ruthenium should be considered as interfered.

Fig. 6 shows small nanoparticles of the ruthenium on the $CeAlO_3$ surface, obtained by heating at 1000 °C in the hydrogen. Calculated particle size distribution indicates that the size of the particles is below 5 nm, but most are smaller than 3 nm. These particles were formed by the ions, which diffuse from the bulk of ceria to the surface, where were reduced by interaction with the hydrogen from the environment [36].

The reduced ruthenium atoms are probably dispersed on the oxide surface as single atoms or clusters, and with increasing temperature, they diffuse on this surface creating metallic nanoparticles. Clusters are probably too small to be detectable using the HRTEM method. Due to the high melting temperature of the metallic ruthenium, this process is limited by low mobility of the reduced metal atoms in the temperature range of 300–800 °C [11]. At higher temperatures, the reaction of ceria with the alumina begins, and $CeAlO_3$ is formed (Fig. 5). Metallic ruthenium atoms or clusters, which were present on the ceria surface before the reaction, stay on the surface of the created aluminate (Fig. 6).

Prolonged reduction in the $H_2$ atmosphere at 800 °C for 3 h reveals very high resistance of Ru doped ceria particles supported on the functionalized $\gamma\text{-}Al_2O_3$ against sintering. As is presented in Table 2, mean crystallite size of ceria increases subtly to ~5 nm. An example of XRD pattern for such sample is presented as Fig. S8 and calculated PSD is presented in Fig. S9 in Supplementary Material. Particles of the metallic ruthenium could not be observed in the HRTEM images, but the existence of this phase is clearly visible as a small and sharp peak near 44° in the XRD pattern (Fig. S8).

Data in Table 2 shows, that $Ru_{0.05}Ce_{0.95}O_{2-y}$ nanoparticles on $\gamma\text{-}Al_2O_3$(fn) are up to 800 °C more stable in the reductive atmosphere than in the air. The average crystallite size of ceria after treatment at 800 °C was 4.7 and 6.9 nm, respectively. Extension of the heating time up to 3h causes the only slight growth of the crystallite size in hydrogen (to 4.9 nm), and noticeable change in the air (growth to 9.4 nm). Treatment at elevated temperatures leads also to severe textural changes. Heating at 1000 °C for 3 h decreased the specific surface area from 119 to 67 $m^2/g$ in the oxidizing atmosphere, and to 59 $m^2/g$ in the reducing

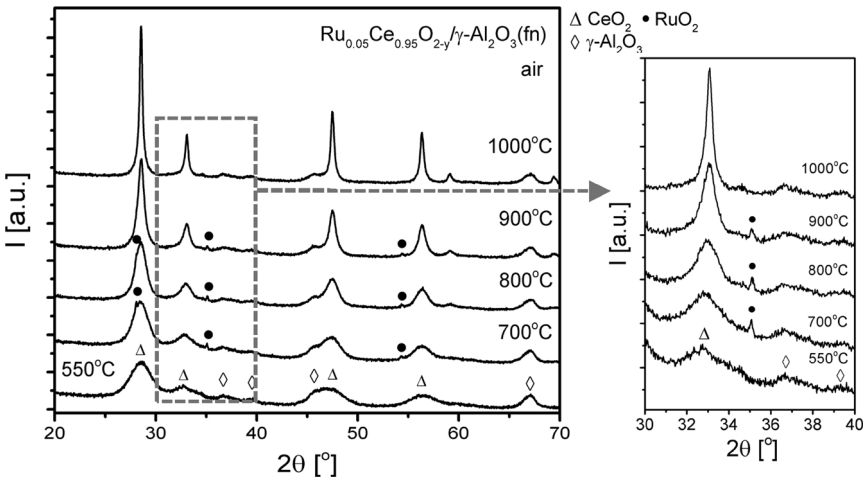


**Fig. 3.** XRD patterns of the $Ru_{0.05}Ce_{0.95}O_{2-y}/\gamma\text{-}Al_2O_3$(fn) after heat treatment at various temperatures in the air for 1 h.

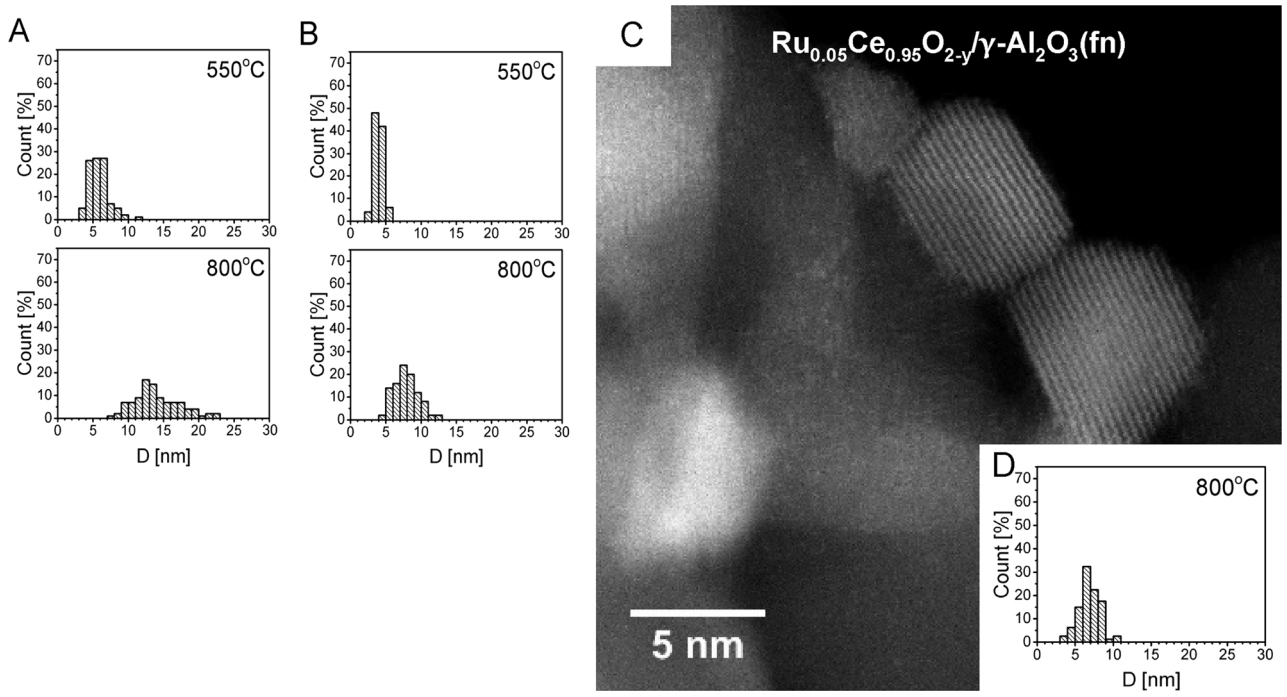


**Fig. 4.** Effect of heat treatment in the air at 800 °C for 3 h on the size distribution of $Ru_{0.05}Ce_{0.95}O_{2-y}$ nanoparticles unsupported (A) and supported on bare alumina (B). C – STEM-HAADF image $Ru_{0.05}Ce_{0.95}O_{2-y}/\gamma\text{-}Al_2O_3$(fn) with PSD (D).

atmosphere. As is visible from Tables 2 and S2, the decline in the surface area can be assigned, in addition to the textural change of the support, also to the growth of ceria particles. In the $H_2$ atmosphere, the change can be also due to the reaction between $CeO_2$ and $Al_2O_3$ with formation of $CeAlO_3$.

### 3.3. Reducibility

#### 3.3.1. $H_2$-TPR

Fig. 7 shows the $H_2$-TPR profiles of $Ru_{0.05}Ce_{0.95}O_{2-y}$ nanoparticles unsupported and supported on bare and functionalized $\gamma\text{-}Al_2O_3$.

At low temperatures (below 200 °C) all samples show very strong reduction feature, that is characteristic for the systems containing precious metals [11,37,38]. From the shape of the TPR profiles it can be supposed, that reduction process of the ruthenium ions consists of at least two steps (maxima at 90 °C, and at 118 °C). The first step origins from easily reducible Ru—O bonds at the surface. The intensity of this peak is low for Ru concentration $x \leq 0.05$ (Fig. S10 – Supplementary material), and increases sharply for $x = 0.075$, when, as was mentioned in chapter 3.1 (cf. also Fig. S3 – Supplementary material), the sample contains $RuO_2$ phase. Therefore, this reduction peak can be due to the presence of Ru oxide phase. The second peak is due to the reduction of the ruthenium ions in the ceria lattice, which forms the Ru-O-Ce bonds [11,21,38,39].

Percentages of ceria reduction in four temperature ranges (up to 200, 500, 850 and 1000 °C) calculated from TPR profiles shown in Fig. 7 are collected as Table 3. Evidently, dispersion of $Ru_{0.05}Ce_{0.95}O_{2-y}$ on the alumina support noticeably increases its reducibility over all temperature ranges. Moreover, the effect is more pronounced (total Ce reduction is 10% higher) for nanoparticles supported on the

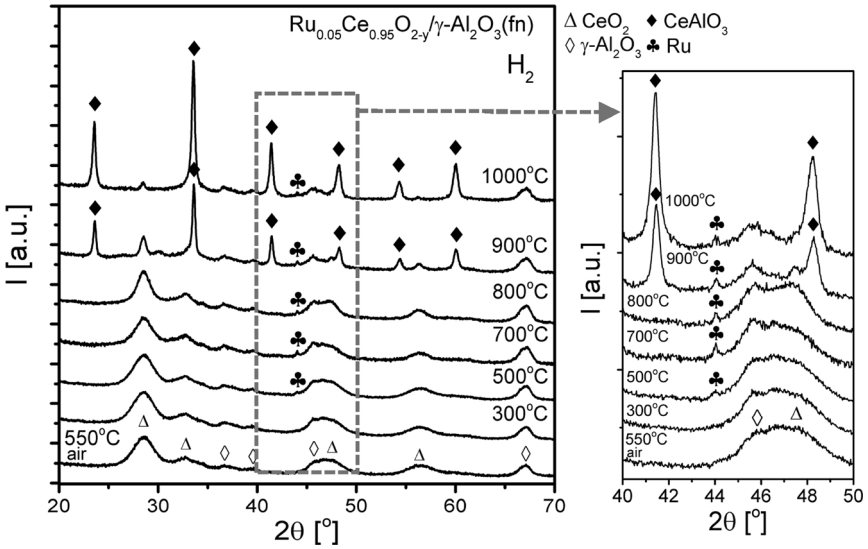


**Fig. 5.** XRD patterns of $Ru_{0.05}Ce_{0.95}O_{2-y}/\gamma\text{-}Al_2O_3$(fn) heated in reducing atmosphere for 1 h. ♦ – reflections corresponding to the tetragonal structure of $CeAlO_3$, ♣ – metallic Ru.

**Table 2**
Average particle sizes calculated for $Ru_{0.05}Ce_{0.95}O_{2-y}/\gamma\text{-}Al_2O_3$(fn) using the full profile Rietveld refinement for samples after heating for 1 h in the oxidizing and reducing atmosphere and the textural properties (specific surface area ($S_{BET}$), total pore volume ($V_{BET}$) and average pore width ($L_{BET}$)) obtained after heating for 3 h.

| T [°C] | Size [nm] | |
|---|---|---|
| | Air | $H_2$ |
| 300 | – | 3.5 |
| 500 | 3.3[a] | 3.7 |
| 700 | 5.1 | 4.3 |
| 800 | 6.9/9.4[b] | 4.7/4.9[b] |
| 900 | 12.1 | 11.2 |
| 1000 | 29.2/29.1[b] | 26.7[b,c] |

| T [°C] | Textural properties | | | | | |
|---|---|---|---|---|---|---|
| | Air | | | $H_2$ | | |
| | $S_{BET}$ [$m^2$/g] | $V_{BET}$ [$cm^3$/g] | $L_{BET}$ [nm] | $S_{BET}$ [$m^2$/g] | $V_{BET}$ [$cm^3$/g] | $L_{BET}$ [nm] |
| as-prepared[a] | 119 | 0.67 | 23 | | – | |
| 800[b] | 82 | 0.62 | 30 | 77 | 0.56 | 29 |
| 1000[b] | 67 | 0.53 | 33 | 59 | 0.55 | 38 |

[a] As-prepared sample, heated in air at 550 °C for 3 h.
[b] Extended treatment for 3 h.
[c] Mean size of the $CeAlO_3$ particles (28.6% wt. of the sample). $CeO_2$ phase is not observed on the XRD pattern.

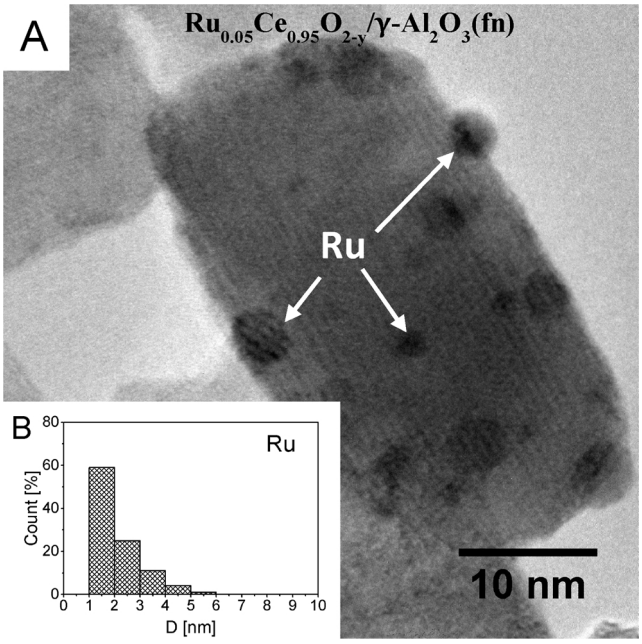


**Fig. 6.** (A) HRTEM of the $Ru_{0.05}Ce_{0.95}O_{2-y}/\gamma\text{-}Al_2O_3$(fn) after heating at 1000 °C in the $H_2$ atmosphere; (B) calculated PSD of the metallic ruthenium nanoparticles on the aluminate surface.

functionalized alumina. A similar effect, which occurred for analogous systems with undoped ceria [6], was attributed to better dispersion of ceria and enhanced the availability of the more reducible atoms on the oxide surface.

For the systems containing ceria doped with ruthenium ions, the $H_2$ uptake in the range up to 200 °C is, however, much higher than that required for total ruthenium reduction. For unsupported $Ru_{0.05}Ce_{0.95}O_{2-y}$ the uptake was 1.05 mmol per gram of the mixed oxide, while 0.6 mmol/g is required to reduce $Ru^{IV}$ to $Ru^{\circ}$. Thus, in this range, a certain amount of cerium must also be reduced. It has been proposed that it could be cerium ions forming weak Ce—O—Ru bonds

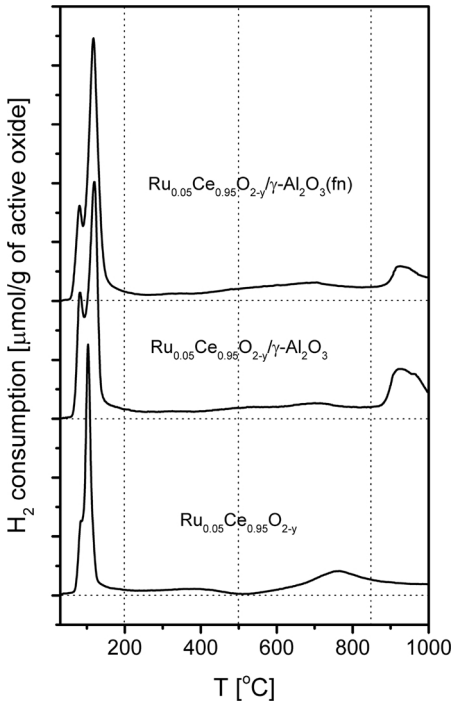


**Fig. 7.** Representative TPR profiles of the as-prepared samples.

**Table 3**
Reduction degree of cerium oxide and hydrogen consumption obtained in the TPR measurements.

| Sample | $Ce^{IV}$ reduction degree [%] | | | | Total $H_2$ consumption [mmol $H_2$/g of active oxide] |
|---|---|---|---|---|---|
| | < 200 °C | < 500 °C | < 850 °C | Total | |
| $CeO_2$ | 0.6/0.03[a] | 6.8/0.40[a] | 23.1 | 28.8 | 1.64 |
| $Ru_{0.05}Ce_{0.95}O_{2-y}$ | 8.9/1.05[a] (0.6)[b] | 13.6/1.3[a] | 17.1 | 32.6 | 2.38 |
| $CeO_2/\gamma\text{-}Al_2O_3$ | 1.1/0.07[a] | 17.6/1.02[a] | 40.4 | 52.0 | 2.92 |
| $Ru_{0.05}Ce_{0.95}O_{2-y}/\gamma\text{-}Al_2O_3$ | 21.6/ 1.80[a] (0.6)[b] | 30.3/2.28[a] | 35.4 | 56.8 | 3.80 |
| $CeO_2/\gamma\text{-}Al_2O_3$(fn) | 0.8/0.05[a] | 18.9/1.10[a] | 42.8 | 60.4 | 3.51 |
| $Ru_{0.05}Ce_{0.95}O_{2-y}/\gamma\text{-}Al_2O_3$(fn) | 26.8/ 2.08[a] (0.6)[b] | 34.5/2.5[a] | 43.8 | 66.6 | 4.30 |

[a] $H_2$ consumption [in mmol $H_2$/g of the active oxide].
[b] $H_2$ consumption [mmol $H_2$/g of active oxide] calculated for the complete reduction of $Ru^{IV}$ to $Ru^{\circ}$ ($RuO_2 + 2H_2 \rightarrow Ru^{\circ} + 2H_2O$).

[31,38,40]. For $Ru_{0.11}Ce_{0.89}O_2$ obtained by Kurnatowska et al. [11], $H_2$ uptake up to 200 °C is 1.66 mmol of $H_2$/g (1.24 mmol/g was calculated as required to reduce $Ru^{IV}$ to $Ru^{\circ}$), what gives very similar cerium reduction. Much higher uptakes are observed for $Ru_{0.05}Ce_{0.95}O_{2-y}/\gamma\text{-}Al_2O_3$ and $Ru_{0.05}Ce_{0.95}O_{2-y}/\gamma\text{-}Al_2O_3$(fn), 1.80 and 2.08 mmol $H_2$/g of the mixed oxide, respectively, corresponding to ~20–30% cerium reduction. In the temperature range up to 500 °C, the $H_2$ consumption for $Ru_{0.05}Ce_{0.95}O_{2-y}/\gamma\text{-}Al_2O_3$(fn) system (2.5 mmol $H_2$/g of mixed oxide) is still two times higher than in unsupported $Ru_{0.05}Ce_{0.95}O_{2-y}$ (1.3 mmol $H_2$/g) [11].

The TPR profiles of ceria and Ru doped ceria nanoparticles supported on alumina (Fig. 7) differ significantly from that of unsupported ceria [6]. For example, the bulk reduction peak, which is observed as a strong maximum at ~800 °C for the undoped ceria [6], occurs as a broad feature at lower temperature if the oxide is supported on alumina [6,8,41]. Furthermore, due to the increase of the content of easily

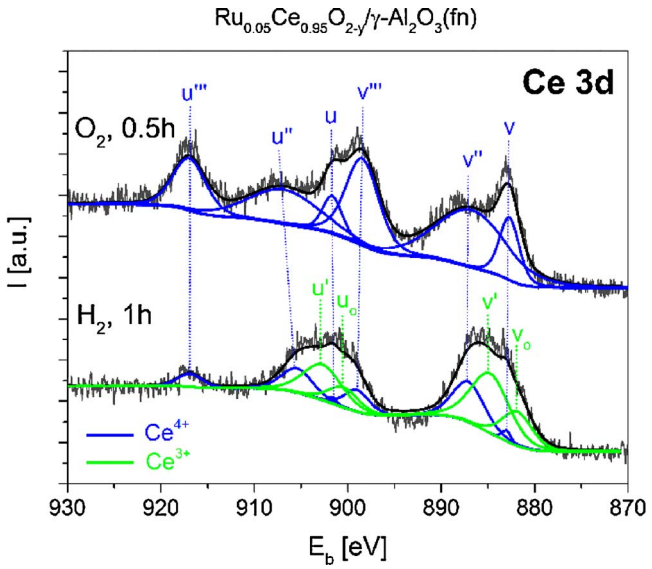


**Fig. 8.** Results of the XPS analysis for $Ru_{0.05}Ce_{0.95}O_{2-y}/\gamma Al_2O_3$(fn) after *in situ* thermal treatments: 500 °C for 30 min in $O_2$ (1 bar), and at 500 °C for 1h in the $H_2$ atmosphere (1 bar) [u''' – $Ce^{4+}3d_{3/2}$, u'' – $Ce^{4+}3d_{3/2}$, u' – $Ce^{3+}3d_{3/2}$, u – $Ce^{4+}3d_{3/2}$, $u_o$ – $Ce^{4+}3d_{3/2}$, v''' – $Ce^{4+}3d_{5/2}$, v'' – $Ce^{4+}3d_{5/2}$, v' – $Ce^{3+}3d_{5/2}$, v – $Ce^{4+}3d_{5/2}$, $v_o$ – $Ce^{3+}3d_{5/2}$].

reducible cerium ions after deposition of the oxide on the alumina support (which increases with the nanoparticles' dispersion), the surface reduction peak (~500 °C) surpasses the bulk reduction one (ref. [6] and Fig. S10 – Supplementary material). Additionally, a new peak occurs at temperatures ~900 °C and is attributed to the formation of a new aluminate phase (Fig. S11 – Supplementary material) [6,35].

### 3.3.2. XPS

The photoelectron spectroscopy is a powerful tool to study cerium containing materials [1]. This method enables analysis of the oxidation state of the cerium ions at the sample surface [42].

However, because of the high susceptibility of the reduced ceria to an oxidation process in air, XPS results obtained for the samples exposed to air may be unreliable. In the present work, the temperature treatments of the samples were performed in the preparation chamber of XPS apparatus, and then the samples were analyzed in a vacuum, without contact with the atmosphere. Unfortunately, due to the low signal/noise ratio caused by the low concentration of ruthenium in the catalyst (Ru content 0.2% at.), analysis of the ruthenium lines was impossible. Fig. 8 presents Ce 3d core level spectra of $Ru_{0.05}Ce_{0.95}O_{2-y}/\gamma$-$Al_2O_3$(fn). Analogous spectra of the reference $CeO_2/\gamma$-$Al_2O_3$(fn) are shown in Fig. S12 (Supplementary material), and the detailed results obtained by the analysis of these spectra are collected in Table S3 (Supplementary material). As expected, the Ce 3d spectrum after treatment in oxygen atmosphere contains only $Ce^{4+}$ lines for both samples. After reduction at 500 °C for 1h, the spectra contain an important contribution from $Ce^{3+}$ ions, given in Table 4. XPS spectra presented are similar to that reported previously in [11,41,43,44].

As appears from Table 4, the percentage of cerium reduction in the $Ru_{0.05}Ce_{0.95}O_{2-y}/\gamma$-$Al_2O_3$(fn) is much higher than in the $CeO_2/\gamma$-$Al_2O_3$(fn), 64% and 44%, respectively. It confirms a promoting role of Ru in the cerium reduction process. As was mentioned previously, it may be due to the presence of Ru—O—Ce bonds. Other reason could be the activation of hydrogen by the metallic Ru, what can facilitate the reduction of cerium. Such effect was observed by Kato et al. for $Pt/CeO_2$ [45].

**Table 4**
The reduction degrees calculated from XPS.

| Sample | $Ce^{IV}$ reduction degree [% of $Ce^{3+}$][a] | |
|---|---|---|
| | $O_2$, 0.5 h, 500 °C | $H_2$, 1 h, 500 °C |
| $CeO_2/\gamma$-$Al_2O_3$(fn) | 0 | 44 |
| $Ru_{0.05}Ce_{0.95}O_{2-y}/\gamma$-$Al_2O_3$(fn) | 0 | 64 |

[a] Calculated as $Ce^{3+}$[%] = 100%·Σ(areas of $Ce^{3+}$ bands)/(Σ(areas of $Ce^{3+}$ bands) + Σ(areas of $Ce^{4+}$ bands)) [44].

The presence of Ru in the ceria lattice enhances the mobility of ions in the structure, what can also facilitate the reduction process. The percentage of $Ce^{3+}$ in the $Ru_{0.05}Ce_{0.95}O_{2-y}/\gamma$-$Al_2O_3$(fn) (64%) is much higher than 15% reported for unsupported $Ce_{0.89}Ru_{0.11}O_2$ reduced at 800° C and exposed to air before XPS measurements. For comparison, Wen et al. reported 40% of $Ce^{3+}$ ions in $Au/CeO_2$ and $Pt/CeO_2$ systems studied by near ambient pressure XPS in 1 Tr $H_2$ at 300 °C [46]. It shows the importance of XPS studies after *in situ* thermal treatments, but also the promoting effect of dispersion of the oxide on the support on the ceria reducibility.

### 3.4. Catalytic activity and stability of the obtained systems in oxidation processes

#### 3.4.1. Soot oxidation

Due to the high reducibility at low temperatures, the obtained systems are promising as catalysts for the oxidation reactions. Kurnatowska et al., found, that unsupported $Ru_{0.11}Ce_{0.95}O_{2-y}$, showed high activity in the soot combustion process ($T_{50}$ = 398 °C, tight contact mode, catalyst/soot weight ratio 2:1) [11]. Also, other Ru containing ceria-based systems were reported as active in this process. Ruthenium impregnated on ceria (5% wt.) and stabilized on the $Al_2O_3$ support, developed by Aouad et al., showed also high activity in this process ($T_{50}$ = 490 °C, tight contact mode, 20/80 soot to catalyst weight ratio) [18].

Results obtained in this work are summarized in Table 5. In order to evaluate the activity and stability of our systems, the process of soot combustion was performed in three successive cycles. Pure soot undergoes half combustion at 591 °C, and the same result was obtained in the presence of $CeO_2/\gamma$-$Al_2O_3$(fn). Results obtained for the $Ru_{0.05}Ce_{0.95}O_{2-y}$ based systems show, that doping of ceria with the ruthenium decreases the soot half-oxidation temperature by about 100 °C. Deposition of $Ru_{0.05}Ce_{0.95}O_{2-y}$ on alumina improves additionally the stability of the catalysts in the successive cycles. For unsupported $Ru_{0.05}Ce_{0.95}O_{2-y}$ the half-oxidation temperature increases significantly in the second and third oxidation cycle, from 488 °C up to 566 °C in the third catalytic cycle. Moreover, in the third oxidation cycle, temperature as high as 650 °C is insufficient to oxidize the whole amount of soot in the system (Fig. S13, Supplementary material). For $Ru_{0.05}Ce_{0.95}O_{2-y}$ nanoparticles on the bare alumina, the $T_{50}$ temperature increases up to 511 °C in the third cycle, while on the functionalized alumina the $T_{50}$ in second and third cycles are the same and equal to 501 °C. Clearly, the novel method of the catalysts synthesis, involving the support functionalization, enables noticeable improvement of the catalyst stability during the catalytic process.

When comparing the results of the activity of catalysts in soot combustion from various groups it is crucial to remember, that contact between the soot and the catalyst and their mass ratio may drastically affect the results. The soot to mixed oxide ratio of 2:1 used in this work is higher than that in [11] (1:2) or [18] (1:4) where lower $T_{50}$ values were obtained, 398 °C and 490 °C, respectively.

To explain the differences in thermal stability of the catalysts in the reaction conditions HRTEM and XRD studies were performed. Fig. 9 presents HRTEM image of $Ru_{0.05}Ce_{0.95}O_{2-y}/\gamma$-$Al_2O_3$(fn) catalyst after third soot oxidation cycle.

It appears that $Ru_{0.05}Ce_{0.95}O_{2-y}$ nanoparticles are still small (≤8 nm), though slightly bigger than in the as-prepared sample (≤5 nm). $Ru_{0.05}Ce_{0.95}O_{2-y}/\gamma$-$Al_2O_3$, and especially unsupported $Ru_{0.05}Ce_{0.95}O_{2-y}$ experience severer structure changes (Fig. S14, S15 in

**Table 5**
Catalytic activity of selected systems in soot and propane combustion measured in 3 successive cycles. Average crystallite sizes calculated from XRD data for samples after third catalytic cycle are presented.

| Sample | $T_{50}$ [°C] soot | | | $D_{XRD}$ [nm] | $T_{50}$ [°C] propane | | | $r_{240}$[a] [mol $g^{-1}$ $min^{-1}$] | $r_{10\%}$[d] [mol $g^{-1}$ $min^{-1}$] | $D_{XRD}$ [nm] |
|---|---|---|---|---|---|---|---|---|---|---|
| | 1 | 2 | 3 | | 1 | 2 | 3 | | | |
| – | 591 | – | – | – | 665 | – | – | 0 | – | – |
| $CeO_2$/ γ-$Al_2O_3$(fn) | 591 | – | – | – | 385 | – | – | 0 | 0.018 | – |
| $Ru_{0.05}Ce_{0.95}O_{2-y}$ | 488 | 518 | 566 | 12.9 | – | – | – | – | – | – |
| $Ru_{0.05}Ce_{0.95}O_{2-y}$/γ-$Al_2O_3$ | 492 | 504 | 511 | 5.3 | 236 | 314 | 315 | 0.15 | 0.017 | 9.6 |
| $Ru_{0.05}Ce_{0.95}O_{2-y}$/γ-$Al_2O_3$(fn) | 487 | 501 | 500 | 4.9 | 225 | 295 | 305 | 0.18 | 0.018 | 8.5 |
| $Co_3O_4$/ZSM-5 | – | – | – | – | 235[b] | – | – | 0.065[b] | 0.0084[b] | – |
| $Co_{2.3}Mn_{0.7}O_4$ | – | – | – | – | 200[c] | – | – | 0.074[c] | 0.0080[c] | – |

[a] Calculated at 240 °C for the first propane oxidation cycle as a mole of propane molecules oxidized in 1 min per gram of the mixed oxide in the catalyst sample. The value was calculated based on the flow rate (v = 100 ml/min), 5000 ppm concentration of propane in the flowing gas, and the specific propane conversion at 240 °C ($r_{240}$) [40]: r [mol $g^{-1}$ $min^{-1}$] = ((Pv/RT) propane conversion at 240 °C)/mass of the active phase [g] = ((1013.25 [hPa] · 0.1 [$dm^3$ $min^{-1}$])/(83.14 [(hPa $dm^3$ $mol^{-1}$ $K^{-1}$] 298.15 [K]) propane conversion at 240 °C)/mass of the active phase [g].
[b] Calculated with parameters from [48].
[c] Calculated with parameters from [49].
[d] $r_{10\%}$ was calculated for the first catalytic cycle using equation from[a], with constant propane conversion of 10% (kinetic regime).

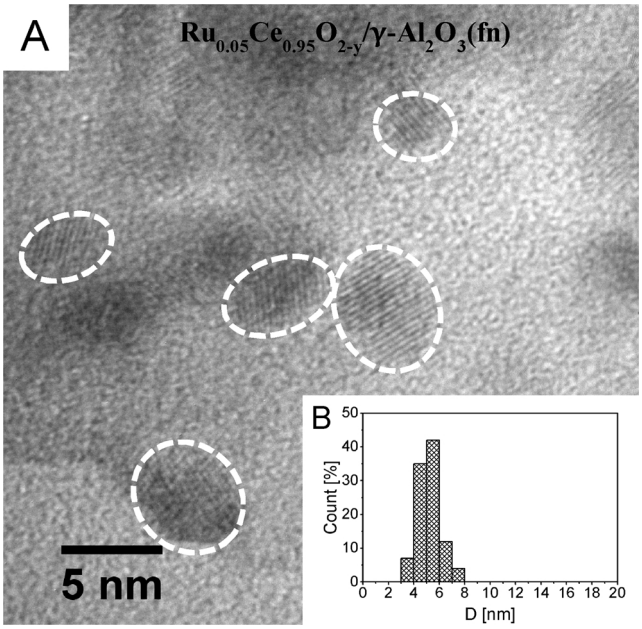


**Fig. 9.** (A) HRTEM image of $Ru_{0.05}Ce_{0.95}O_{2-y}$/γ-$Al_2O_3$(fn) for the sample after third soot oxidation cycle conducted up to 650 °C; (B) PSD of the active nanoparticles in the sample calculated from the HRTEM.

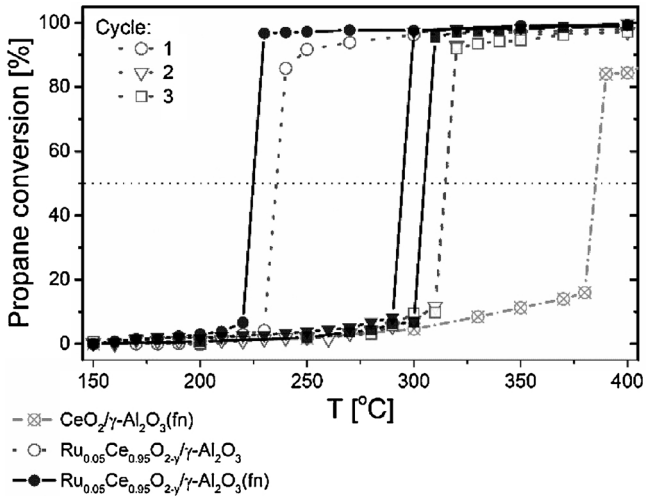


**Fig. 10.** Catalytic propane oxidation for $Ru_{0.05}Ce_{0.95}O_{2-y}$ deposited on bare or functionalized alumina. Results obtained in three catalytic cycles. For comparison, the result obtained for the reference $CeO_2$/γ-$Al_2O_3$(fn) sample in the first cycle is presented.

the Supplementary material). The particle size after three reaction cycles was 2–12 and 5–18 nm, respectively. These results undoubtedly confirm the positive influence of the alumina functionalization on the stability of $Ru_xCe_{1-x}O_{2-y}$/γ-$Al_2O_3$ catalysts. The microscopic results correspond well with the XRD data (Table 5, Fig. S15). The average particle sizes for oxides unsupported, supported on bare and functionalized alumina are 12.9, 5.3 and 4.9 nm, respectively. After the third cycle, for each studied catalyst, a substantial part of the ruthenium ions is located outside the ceria lattice as $RuO_2$ phase (Fig. S15).

### 3.4.2. Propane oxidation

Results on the catalytic oxidation of propane are summarized in Fig. 10 and in Table 5. It is seen that $Ru_{0.05}Ce_{0.95}O_{2-y}$/γ-$Al_2O_3$(fn) sample is by far the most active in the reaction ($T_{50}$ in the first catalytic cycle is equal to 225 °C). For $Ru_{0.05}Ce_{0.95}O_{2-y}$ deposited on bare alumina, the $T_{50}$ is 11 °C higher. Moreover, the former catalyst achieves very high propane conversion (> 90%) already at 230 °C, as compared to 250 °C for the latter. Total ~100% conversion is obtained at ~240 °C for $Ru_{0.05}Ce_{0.95}O_{2-y}$/γ-$Al_2O_3$(fn), and 92% for doped ceria on bare alumina. Propane half-combustion temperature for the undoped ceria was significantly higher ($T_{50}$ = 385 °C), what proves the improvement of the activity for the system after doping with ruthenium ions.

The activity of both studied doped ceria catalysts declines in the successive reaction cycles. In the second cycle, $T_{50}$ increases by 70 and 79 °C for ceria deposited on functionalized and bare alumina, respectively. The growth of $T_{50}$ in the third cycle is smaller (10 and 1 °C).

Results obtained in this work may be compared with those reported in the literature for active oxide catalysts. Zhu et al. [48] developed $Co_3O_4$/zeolite catalyst with the half-oxidation temperature $T_{50}$ = 235 °C (200 mg of catalyst in the gas mixture containing 2000 ppm of propane and 2% of $O_2$ in $N_2$, gas flow = 100 $cm^3$/min). Another example is $Co_{2.3}Mn_{0.7}O_4$ catalyst developed by Faure et.al. [49], $T_{50}$ = 200 °C (50 mg of the catalyst in the gas mixture containing 0.4% of propane in Ar with 20% of O2, gas flow ~100 $cm^3$/min).

Comparison of the catalytic performance of various systems in the propane oxidation process should be done cautiously, taking into account the influence of the catalyst mass and process parameters on the catalytic behavior. For example, an increase of the mass of the active component of the catalyst (in our case ~25% wt. of the sample present in the reactor) or decrease of the propane concentration in the feed gas can significantly enhance the propane conversion obtained at the same temperature. Thus, the kinetic parameter of the compared systems was

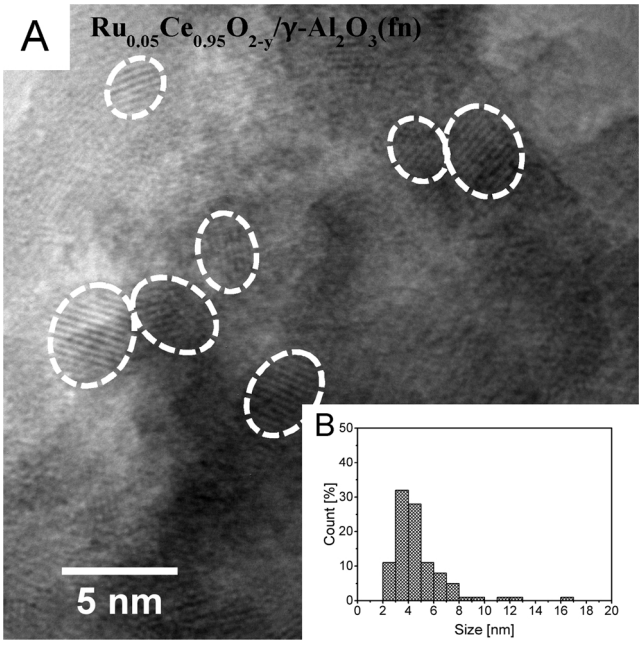


**Fig. 11.** (A) HRTEM image of $Ru_{0.05}Ce_{0.95}O_{2-y}/\gamma$-$Al_2O_3$(fn) for the sample after third propane oxidation cycle conducted up to 400 °C; (B) PSD of the active nanoparticles in the sample calculated from the HRTEM.

calculated for the experimental or literature data at the same selected temperature (240 °C), as well as in the kinetic regime of the studied process (at the 10% conversion of propane) and the obtained results are collected in Table 5. The first parameter was determined to enable comparison of different catalytic systems at the same temperature, and the second to compare at the conditions, at which the diffusion limitations are absent. It is clearly visible, that in the first catalytic oxidation cycle, the $Ru_{0.05}Ce_{0.95}O_{2-y}/\gamma$-$Al_2O_3$(fn) system exhibits the highest specific rate of the reaction (0.18 mol $g^{-1}$ $min^{-1}$), in comparison with the reference sample containing bare alumina (0.15 mol $g^{-1}$ $min^{-1}$), as well as in comparison with the results known from the literature for the other oxide catalytic systems [48,49].

It should be noticed that the oxide catalysts are less active in propane oxidation process than the catalysts contained precious metals ($T_{50}$ < 200 °C) [19], and are very rarely used for this process. Searching for the active oxide catalysts for this process is, however, justified for economic reasons.

Figs. 11 and S16 (Supplementary material) depict the effect of three cycles of the propane oxidation process on the morphology of the catalysts. For $Ru_{0.05}Ce_{0.95}O_{2-y}$ deposited on the functionalized alumina slight broadening of the PSDs is observed, but still prevailing part of the nanoparticles have sizes ≤ 5 nm, and similar results were obtained for sample deposited on bare alumina (Fig. S16). These results correlate well with the XRD data (Table 5), where the obtained mean particle size is equal to 8.5 nm, and 9.6 nm for oxide deposited on functionalized and bare alumina. The stabilizing effect of the particles on the functionalized support was therefore also noticed during this process. The visible difference in catalytic behavior can be due to the fact, that in the $Ru_{0.05}Ce_{0.95}O_{2-y}/\gamma$-$Al_2O_3$(fn) sample, the active particles exist mostly as single units (Fig. 1). In such system, the amount of available active surface of the catalyst is therefore significantly higher, than in the system with bare alumina, where the particles are agglomerated (Fig. S6). As for the catalysts after soot oxidation, in the systems after third propane combustion process, ruthenium exists mostly as $RuO_2$ (Fig. S17).

## 4. Conclusions

In this work, highly dispersed, very stable and active catalytic systems were synthesized *via* a new, original method. $Ru_xCe_{1-x}O_{2-y}$ (x = 0.025, 0.05, 0.075) nanoparticles (< 5 nm) deposited on alumina functionalized with a monolayer of decanoic acid are more stable under an oxidizing atmosphere and especially in the reductive atmosphere up to 800 °C, than the reference systems with bare alumina or unsupported systems. Heating for 3 h in the air at 800 °C increased the mean particle size to ~9 nm, whereas heating in the reductive atmosphere ($H_2$), only up to ~5 nm, proving excellent resistance of the systems against sintering at these conditions.

As was confirmed by the XPS and $H_2$-TPR methods, doping with Ru enhances significantly the reducibility of ceria particles stabilized on an alumina support, in the low-temperature range, crucial for catalytic activity in oxidizing reactions. Using of the functionalized support provides additional enhancement of the reducibility by about 10%. The samples are very active in soot ($T_{50}$ = 487–500 °C) and propane oxidation ($T_{50}$ = 225–305 °C) and show high stability in successive cycles of the catalytic processes.

## Acknowledgments

The authors wish to thank: Mrs. Z. Mazurkiewicz for a valuable help with the sample preparation, Mrs. E. Bukowska for the XRD measurements, Dr. M. Ptak, Ms. A. Ciupa and Dr. R. Szukiewicz (EIT+) for the Raman, FTIR and XPS spectra recording, Mr. P. Kraszkiewicz and Prof. M. Zawadzki for the help with $H_2$-TPR and catalytic propane oxidation tests measurements.

## Appendix A. Supplementary data

Supplementary material related to this article can be found, in the online version, at doi:https://doi.org/10.1016/j.apcatb.2018.02.037.

## References

[1] D.R. Mullins, The surface chemistry of cerium oxide, Surf. Sci. Rep. 70 (2015) 42–85, http://dx.doi.org/10.1016/j.surfrep.2014.12.001.
[2] A. Trovarelli, Catalytic properties of ceria and $CeO_2$ – containing materials, Catal. Rev. 38 (1996) 439–520, http://dx.doi.org/10.1080/01614949608006464.
[3] T. Montini, M. Melchionna, M. Monai, P. Fornasiero, Fundamentals and catalytic applications of $CeO_2$ – based materials, Chem. Rev. 116 (2016) 5987–6041, http://dx.doi.org/10.1021/acs.chemrev.5b00603.
[4] J. Paier, C. Penschke, J. Sauer, Oxygen defects and surface chemistry of ceria: Quantum chemical studies compared to experiment, Chem. Rev. 113 (2013) 3949–3985, http://dx.doi.org/10.1021/cr3004949.
[5] C. Walkey, S. Das, S. Seal, J. Erlichman, K. Heckman, L. Ghibelli, E. Traversa, J.F. McGinnis, W.T. Self, Catalytic properties and biomedical applications of cerium oxide nanoparticles, Environ. Sci. Nano 2 (2015) 33–53, http://dx.doi.org/10.1039/C4EN00138A.
[6] K.A. Ledwa, L. Kępiński, Dispersion of ceria nanoparticles on γ-alumina surface functionalized using long chain carboxylic acids, Appl. Surf. Sci. 400 (2017) 212–219, http://dx.doi.org/10.1016/j.apsusc.2016.12.127.
[7] M. Trueba, S.P. Trasatti, γ-Alumina as a support for catalysts: a review of fundamental aspects, Eur. J. Inorg. Chem. (2005) 3393–3403, http://dx.doi.org/10.1002/ejic.200500348.
[8] J.Z. Shyu, W.H. Weber, H.S. Gandhi, Surface characterization of alumina-supported ceria, J. Phys. Chem. 92 (1988) 4964–4970.
[9] A. Martinez-Arias, M. Fernandez-Garcia, L.N. Salamanca, R.X. Valenzuela, J.C. Conesa, J. Soria, Structural and redox properties of ceria in alumina-supported ceria catalyst supports, J. Phys. Chem. B 104 (2000) 4038–4046, http://dx.doi.org/10.1021/jp992796y.
[10] M.I. Zaki, G.A.M. Hussein, S.A.A. Mansour, H.M. Ismail, G.A.H. Mekhemer, Ceria on silica and alumina catalysts: dispersion and surface acid-base properties as probed by X-ray diffractometry, UV–Vis diffuse reflectance and in situ IR absorption studies, Colloids Surf. A Physicochem. Eng. Asp. 127 (1997) 47–56, http://dx.doi.org/10.1016/S0927-7757(96)03943-X.
[11] M. Kurnatowska, W. Mišta, P. Mazur, L. Kępiński, Nanocrystalline $Ce_{1-x}Ru_xO_2$ – microstructure, stability and activity in CO and soot oxidation, Appl. Catal. B Environ. 148–149 (2014) 123–135, http://dx.doi.org/10.1016/j.apcatb.2013.10.047.
[12] M. Kurnatowska, L. Kępiński, Structure and thermal stability of nanocrystalline $Ce_{1-x}Rh_xO_{2-y}$ in reducing and oxidizing atmosphere, Mater. Res. Bull. 48 (2013)

852–862, http://dx.doi.org/10.1016/j.materresbull.2012.11.076.
[13] P. Bera, M.S. Hegde, Noble metal ions in $CeO_2$ and $TiO_2$: synthesis, structure and catalytic properties, RSC Adv. 5 (2015) 94949–94979, http://dx.doi.org/10.1039/C5RA16474E.
[14] P. Bera, S.T. Aruna, Solution combustion synthesis, characterization and catalytic properties of oxide materials, in: B. Sels, M.V. de Voorde (Eds.), Nanotechnol. Catal. Appl. Chem. Ind. Energy Res. Environ. Prot., First, Wiley, Weinheim, 2017, pp. 91–117.
[15] M.S. Hegde, P. Bera, Noble metal ion substituted $CeO_2$ catalysts: electronic interaction between noble metal ions and $CeO_2$ lattice, Catal. Today 253 (2015) 40–50, http://dx.doi.org/10.1016/j.cattod.2015.03.035.
[16] O. Mendiuk, M. Nawrocki, L. Kępiński, The synthesis of $Ce_{1-x}Ln_xO_{2-y}$ (Ln = Pr, Sm, Gd, Tb) nanocubes by hydrothermal methods, Ceram. Int. 42 (2016) 1998–2012, http://dx.doi.org/10.1016/j.ceramint.2015.10.006.
[17] M. Cargnello, J.J. Delgado Jaén, J.C. Hernández Garrido, K. Bakhmutsky, T. Montini, J.J. Calvino Gámez, R.J. Gorte, P. Fornasiero, Exceptional activity for methane combustion over modular Pd@$CeO_2$ subunits on functionalized $Al_2O_3$, Science 337 (2012) 713–717, http://dx.doi.org/10.1126/science.1222887.
[18] S. Aouad, E. Saab, E. Abi Aad, A. Aboukaïs, Reactivity of Ru – based catalysts in the oxidation of propene and carbon black, Catal. Today 119 (2007) 273–277, http://dx.doi.org/10.1016/j.cattod.2006.08.030.
[19] K. Baranowska, J. Okal, Bimetallic Ru-Re/$\gamma$-$Al_2O_3$ catalysts for the catalytic combustion of propane: effect of the Re addition, Appl. Catal. A Gen. 499 (2015) 158–167, http://dx.doi.org/10.1016/j.apcata.2015.04.023.
[20] S. Pradhan, D.C. Upham, H. Metiu, E.W. McFarland, Partial oxidation of propane with $CO_2$ on Ru doped catalysts, Catal. Sci. Technol. 6 (2016) 5483–5493, http://dx.doi.org/10.1039/C6CY00011H.
[21] P. Singh, M.S. Hegde, $Ce_{1-x}Ru_xO_{2-\delta}$ (x = 0.05, 0.10): A new high oxygen storage material and Pt, Pd-free three-way catalyst, Chem. Mater. 21 (2009) 3337–3345, http://dx.doi.org/10.1021/cm900875s.
[22] J. Okal, M. Zawadzki, Catalytic combustion of butane on Ru/$\gamma$-$Al_2O_3$ catalysts, Appl. Catal. B Environ. 89 (2009) 22–32, http://dx.doi.org/10.1016/j.apcatb.2008.11.024.
[23] C.S. Chang, S.Y. Suen, Modification of porous alumina membranes with n-alkanoic acids and their application in protein adsorption, J. Membr. Sci. 275 (2006) 70–81, http://dx.doi.org/10.1016/j.memsci.2005.09.005.
[24] S. Damyanova, C.A. Perez, M. Schmal, J.M.C. Bueno, Characterization of ceria-coated alumina carrier, Appl. Catal. A Gen. 234 (2002) 271–282, http://dx.doi.org/10.1016/S0926-860X(02)00233-8.
[25] P. Singh, N. Mahadevaiah, S.K. Parida, M.S. Hegde, A non-deactivating, non-platinum catalyst for water gas shift reaction, J. Chem. Sci. 123 (2011) 577–592.
[26] S. Sharma, Z. Hu, P. Zhang, E.W. McFarland, H. Metiu, $CO_2$ methanation on Ru-doped ceria, J. Catal. 278 (2011) 297–309, http://dx.doi.org/10.1016/j.jcat.2010.12.015.
[27] Y. Li, X. Wang, Y. Shao, D. Tang, B. Wu, Z. Tang, W. Lin, Stability and spinodal decomposition of the solid-solution phase in the ruthenium–cerium–oxide electrocatalyst, Phys. Chem. Chem. Phys. 17 (2015) 1156–1164, http://dx.doi.org/10.1039/C4CP04131C.
[28] M. Stojmenović, M. Žunić, J. Gulicovski, V. Dodevski, M. Prekajski, A. Radulović, S. Mentus, Structural, morphological and electrical properties of $Ce_{1-x}Ru_xO_{2-\delta}$ (x = 0.005–0.02) solid solutions, Ceram. Int. 42 (2016) 14011–14020, http://dx.doi.org/10.1016/j.ceramint.2016.06.007.
[29] F. Wang, C. Li, X. Zhang, M. Wei, D.G. Evans, X. Duan, Catalytic behavior of supported Ru nanoparticles on the {100}, {110}, and {111} facet of $CeO_2$, J. Catal. 329 (2015) 177–186, http://dx.doi.org/10.1016/j.jcat.2015.05.014.
[30] A. Satsuma, M. Yanagihara, J. Ohyama, K. Shimizu, Oxidation of CO over Ru/Ceria prepared by self-dispersion of Ru metal powder into nano-sized particle, Catal. Today 201 (2013) 62–67, http://dx.doi.org/10.1016/j.cattod.2012.03.048.
[31] H. Huang, Q. Dai, X. Wang, Morphology effect of Ru/$CeO_2$ catalysts for the catalytic combustion of chlorobenzene, Appl. Catal. B Environ. 158–159 (2014) 96–105, http://dx.doi.org/10.1016/j.apcatb.2014.01.062.
[32] Q. Dai, S. Bai, X. Wang, G. Lu, Catalytic combustion of chlorobenzene over Ru-doped ceria catalysts: mechanism study, Appl. Catal. B Environ. 129 (2013) 580–588, http://dx.doi.org/10.1016/j.apcatb.2012.10.006.
[33] S. Hosokawa, M. Taniguchi, K. Utani, H. Kanai, S. Imamura, Affinity order among noble metals and $CeO_2$, Appl. Catal. A Gen. 289 (2005) 115–120, http://dx.doi.org/10.1016/j.apcata.2005.04.048.
[34] A.S. Prakash, C. Shivakumara, M.S. Hegde, Single step preparation of $CeO_2$/$CeAlO_3$/ $\gamma$-$Al_2O_3$ by solution combustion method: phase evolution, thermal stability and surface modification, Mater. Sci. Eng. B Solid-State Mater. Adv. Technol. 139 (2007) 55–61, http://dx.doi.org/10.1016/j.mseb.2007.01.034.
[35] A. Piras, A. Trovarelli, G. Dolcetti, Remarkable stabilization of transition alumina operated by ceria under reducing and redox conditions, Appl. Catal. B Environ. 28 (2000) 77–81, http://dx.doi.org/10.1016/S0926-3373(00)00226-5.
[36] S. Imamura, I. Fukuda, S. Ishida, Wet oxidation catalyzed by ruthenium supported on cerium(IV) oxides, Ind. Eng. Chem. Res. 27 (1988) 718–721, http://dx.doi.org/10.1021/ie00076a033.
[37] S. Imamura, Y.-I. Taniguchi, Y. Ikeda, S. Hosokawa, H. Kanai, H. Ando, Reduction behavior of Ru/$CeO_2$ catalysts and their activity for wet oxidation, React. Kinet. Catal. Lett. 76 (2002) 201–206, http://dx.doi.org/10.1023/A:1016572506253.
[38] S. Hosokawa, H. Kanai, K. Utani, Y.I. Taniguchi, Y. Saito, S. Imamura, State of Ru on $CeO_2$ and its catalytic activity in the wet oxidation of acetic acid, Appl. Catal. B Environ. 45 (2003) 181–187, http://dx.doi.org/10.1016/S0926-3373(03)00129-2.
[39] S. Sharma, Z. Hu, P. Zhang, E.W. McFarland, H. Metiu, $CO_2$ methanation on Ru-doped ceria, J. Catal. 278 (2011) 297–309, http://dx.doi.org/10.1016/j.jcat.2010.12.015.
[40] S. Aouad, E. Abi-Aad, A. Aboukaïs, Simultaneous oxidation of carbon black and volatile organic compounds over Ru/$CeO_2$ catalysts, Appl. Catal. B Environ. 88 (2009) 249–256, http://dx.doi.org/10.1016/j.apcatb.2008.10.002.
[41] M.C. Spadaro, S. D'Addato, G. Gasperi, F. Benedetti, P. Luches, V. Grillo, G. Bertoni, S. Valeri, Morphology, structural properties and reducibility of size-selected $CeO_{2-x}$ nanoparticle films, Beilstein J. Nanotechnol. 6 (2015) 60–67, http://dx.doi.org/10.3762/bjnano.6.7.
[42] D.R. Mullins, S.H. Overbury, D.R. Huntley, Electron spectroscopy of single crystal and polycrystalline cerium oxide surface, Surf. Sci. 409 (1998) 307–319, http://dx.doi.org/10.1016/S0039-6028(98)00257-X.
[43] C. Anandan, P. Bera, XPS studies on the interaction of $CeO_2$ with silicon in magnetron sputtered $CeO_2$ thin films on Si and $Si_3N_4$ substrates, Appl. Surf. Sci. 283 (2013) 297–303, http://dx.doi.org/10.1016/j.apsusc.2013.06.104.
[44] P. Bera, C. Anandan, XRD and XPS studies of room temperature spontaneous interfacial reaction of $CeO_2$ thin films on Si and $Si_3N4$ substrates, RSC Adv. 4 (2014) 62935–62939, http://dx.doi.org/10.1039/C4RA09882J.
[45] S. Kato, M. Ammann, T. Huthwelker, C. Paun, M. Lampimäki, M.-T. Lee, M. Rothensteiner, J.A. van Bokhoven, Quantitative depth profiling of $Ce^{3+}$ in Pt/$CeO_2$ by in situ high-energy XPS in a hydrogen atmosphere, Phys. Chem. Chem. Phys. 17 (2015) 5078–5083, http://dx.doi.org/10.1039/C4CP05643D.
[46] C. Wen, Y. Zhu, Y. Ye, S. Zhang, F. Cheng, Y. Liu, P. Wang, F. Tao, Water-gas shift reaction on metal nanoclusters encapsulated in mesoporous ceria studied with ambient-pressure X-ray photoelectron spectroscopy, ACS Nano 6 (2012) 9305–9313, http://dx.doi.org/10.1021/nn303901q.
[48] Z. Zhu, G. Lu, Z. Zhang, Y. Guo, Y. Guo, Y. Wang, Highly active and stable $Co_3O_4$/ZSM-5 catalyst for propane oxidation: Effect of the preparation method, ACS Catal. 3 (2013) 1154–1164, http://dx.doi.org/10.1021/cs400068v.
[49] B. Faure, P. Alphonse, Co-Mn-oxide spinel catalysts for CO and propane oxidation at mild temperature, Appl. Catal. B Environ. 180 (2015) 715–725, http://dx.doi.org/10.1016/j.apcatb.2015.07.019.

## Further reading

H. Zhu, Z. Ma, J.C. Clark, Z. Pan, S.H. Overbury, S. Dai, Low-temperature CO oxidation on Au/fumed $SiO_2$-based catalysts prepared from $Au(en)_2Cl_3$ precursor, Appl. Catal. A Gen. (2007) 326 89–99, doi:10.1016/j.apcata.2007.04.004.